DEVELOPMENT OF INSTRUMENTATION AND METHODS FOR POSITRON SPECTROSCOPY OF DEFECTS IN SEMICONDUCTORS

Jaani Nissilä

Laboratory of Physics
Helsinki University of Technology

Fysiikan laboratorio
Teknillinen korkeakoulu

DISSERTATION 113 (2001)

DEVELOPMENT OF INSTRUMENTATION AND METHODS FOR POSITRON SPECTROSCOPY OF DEFECTS IN SEMICONDUCTORS

Jaani Nissilä

Laboratory of Physics
Helsinki University of Technology
Espoo, Finland

Dissertation for the degree of Doctor of Science in Technology to be presented with due permission of the Department of Engineering Physics and Mathematics for public examination and debate in Auditorium E at Helsinki University of Technology (Espoo, Finland) on the 1st of June, 2001, at 13 o'clock.

Dissertations of Laboratory of Physics, Helsinki University of Technology
ISSN 1455-1802

Dissertation 113 (2001):
Jaani Nissilä: Development of Instrumentation and Methods for Positron Spectroscopy of Defects in Semiconductors
ISBN 951-22-5467-0 (print)
ISBN 951-22-5468-9 (electronic)

OTAMEDIA OY
ESPOO 2001

Abstract

Instrumentation and methods for positron annihilation spectroscopy of point defects in semiconductors have been developed. In particular, techniques to enhance the stability of positron lifetime spectrometers have been investigated. The ageing of the photomultiplier tubes (PMT) of the scintillation detectors can be slowed down by lowering the operating voltages over the PMTs and by compensating the lower gain with fast preamplifiers. The timing characteristics of the apparatus are preserved if the voltages in the input electron optics of the PMTs are high enough and the pulse amplitudes above some tens of millivolts. A positron lifetime spectrometer stabilized against fast inherent drifts in time zero is constructed. An artificial time reference peak in the lifetime spectrum is produced by feeding light pulses from a light-emitting diode onto the photomultipliers via optical fibers of different lengths. The reference peak serves as a basis of stabilization in a digitally stabilized multichannel analyzer.

Positron thermalization in Si and GaAs at low temperatures (8-100 K) is investigated both by experiments and theoretical calculations. Thermalization in GaAs is observed to be noticeably slower than in Si. The mass density of a material is found to play an important role in thermalization since the positron scattering rate off longitudinal-acoustic phonons is inversely proportional to it.

Point defects have been investigated by positron annihilation spectroscopy in Si and CdF_2. V-As and V-P pairs are observed in electron-irradiated silicon. Native V-As_3 complexes are found to be formed when the As-concentration exceeds 10^{20} cm^{-3}. The ionization level $V_2^{-2/-}$ of the silicon divacancy is detected at $E_c - 0.40$ eV by measurements under illumination with monochromatic light. An open-volume defect is observed to be a constituent of the deep-state atomic configurations of the bistable donors In and Ga in CdF_2. The size of the open volume is at least half of a Cd monovacancy.

Preface

This thesis has been prepared in the Laboratory of Physics at Helsinki University of Technology. I wish to express my gratitude to Professor Pekka Hautojärvi for giving me the opportunity to work in his excellent experimental group. I will always remember these years with positive feelings. The invaluable discussions on physics, and life in general, and his encouragement and patience have been essential for the completion of this work.

I am deeply indebted to my advisor, Professor Kimmo Saarinen, for his guidance and encouragement during these years. Kimmo's thirst for understanding physics, and ability to do so, is simply admirable. Sometimes he has also been able to pass some of this on to me, at least I have usually felt much happier when leaving his office than when entering it. And this has happened hundreds, if not thousands, of times.

My sincerest thanks are also due to Dr. Klaus Rytsölä. His role in the technical projects of this thesis has been quintessential. Working with him has always been enjoyable and productive. His advice and criticism have been precious. Typically, also when leaving his office, I have rushed away filled with enthusiasm.

I acknowledge the theoretical group of the laboratory, especially Professors Risto Nieminen and Martti Puska for many fruitful discussions during these years. Dr. Mikko Hakala also deserves thanks for collaboration and useful discussions.

Working with easy-going, talented and enthusiastic colleagues in the experimental positron group has always been most pleasant. I wish to express my warm thanks particularly to Dr. Sirpa Kuisma, Dr. Hannu Kauppinen, Dr. Tatu Laine, Kim Fallström and Antti Laakso, for everything. The joy that you have brought to the everyday life will stay in my mind forever. Collaboration and friendship with Juha Oila, Mikko Karppinen and Sanna Arpiainen are also gratefully acknowledged. During the latest stages of this work, Lauri Salminen as a like-minded and bright person has cheered up my days enormously. For that I am deeply thankful.

The skilful work in the electronic and mechanical workshops has been crucial for the progress of this thesis. Mr. Kaarle Tahvanainen, Mr. Heikki Vaalte and Mr. Eero Turtiainen are gratefully acknowledged. Mrs. Eija Järvinen in the office of the laboratory deserves my warmest thanks for help in various practical issues. In addition, I would like to thank the entire personnel of the laboratory for creating a relaxed and inspirational atmosphere.

The financial support by the Vilho, Yrjö and Kalle Väisälä Foundation and the Jenny and Antti Wihuri Foundation is gratefully acknowledged.

Finally, my heartfelt thanks belong to my family. The importance of the encouragement and support by my parents throughout my life cannot be overestimated. The values I inherited from them have, and will always have, a most important role in my life. Last but certainly not least, I want to express my dearest thanks to Erja for the love and patience that she has given to me irrespective of my long days at work.

Otaniemi, March 2001
Jaani Nissilä

Contents

List of publications

This thesis consists of an overview and the following publications:

I. J. Nissilä, K. Rytsolä, K. Saarinen, and P. Hautojärvi, *Successful implementation of fast preamplifiers in a positron lifetime spectrometer*, submitted for publication in Nuclear Instruments and Methods A.

II. J. Nissilä, M. Karppinen, K. Rytsölä, J. Oila, K. Saarinen, and P. Hautojärvi, *The stabilization of a positron lifetime spectrometer with a high-accuracy time reference*, Nuclear Instruments and Methods A, in print.

III. J. Nissilä, K. Saarinen, and P. Hautojärvi, *Positron thermalization in Si and GaAs*, Physical Review B **63**, 165202 (2001).

IV. K. Saarinen, J. Nissilä, H. Kauppinen, M. Hakala, M. J. Puska, P. Hautojärvi, and C. Corbel *Identification of Vacancy-Impurity Complexes in Highly n-Type Si*, Physical Review Letters **82**, 1883 (1999).

V. H. Kauppinen, C. Corbel, J. Nissilä, K. Saarinen, and P. Hautojärvi, *Photoionization of the silicon divacancy studied by positron-annihilation spectroscopy*, Physical Review B **57**, 12911 (1998).

VI. J. Nissilä, K. Saarinen, P. Hautojärvi, A. Suchocki, and J. M. Langer, *Universality of the Bond-Breaking Mechanism in Defect Bistability: Observation of Open Volume in the Deep States of In and Ga in CdF_2*, Physical Review Letters **82**, 3276 (1999).

The roman numerals are used in this overview when referring to the publications.

The author's contribution

The author has had an active role in all stages of the work reported in this thesis. He has designed and constructed many of the apparatuses used in the experiments. The work presented in papers I, II, III and VI has been under the responsibility of the author and he has also written the publications. All the data reported in paper IV and most of the data in paper V have been measured by him, and he has also actively contributed to the planning of the experiments, analyzing the data and writing of the papers. The author acknowledges the theory group of the laboratory for providing the theoretical results presented in Publications IV and VI.

1 Introduction

The famous Moore's law states that the number of transistors in a microprocessor doubles every two years. This trend has already manifested itself for decades. Now that the dimensions of the components are approaching the scale of the lattice constant, the continuation of the trend is threatened. Namely, with decreasing dimensions, the conductivity and thereby the active carrier concentrations should increase. In silicon, the increase has, however, been prevented by the formation of deactivating point defect complexes [1]. For the industry to be able to overcome these problems, identification of the defects is essential. The investigation of the defects appearing in heavily-doped Si is also one of the subjects of this thesis.

Point defects influence the electrical and optical properties of semiconductors. This is due to the localized states that they create in the energy gap of the material. Point defects play an essential role also in the diffusion of dopant atoms. In many cases, they are very useful (e.g. doping), but they may also be detrimental by acting as recombination or scattering centers.

Positron annihilation spectroscopy (PAS) is a technique that has been used to investigate defects in semiconductors for two decades [2, 3, 4]. It is a nondestructive method which is able to yield unambiguous information about open-volume type defects. In contrast with many common defect spectroscopies, like infra-red absorption spectroscopy (IR), deep level transient spectroscopy (DLTS), etc., a signal attributable to a vacancy cannot arise from any other type of point defects, like antisites or interstitials. This is the asset of PAS. Another advantage of the method is that it can be applied to specimens of any type of conductivity. The weakness of the technique is that positive defects escape detection.

In this thesis, positron annihilation spectroscopies have further been developed for defect studies in semiconductors. In semiconductors, the annihilation characteristics in different defects are often rather similar [2, 3, 4]. To improve the chances of succesfully resolving the experimental data, good statistics is of utmost importance. Therefore, efficient spectrometers with good stability are desired. Publications I and II of this thesis are devoted to the enhancement of the stability of the lifetime spectrometers. Two aspects of instability were treated. Firstly, it was found that the ageing of the photomultiplier tubes (PMT) in the detectors can be slowed down by lowering the supply voltage over the tubes and by compensating the reduced gain with fast preamplifiers. With this action, the average anode current in the PMTs causing the degradation of the gain can be lowered by a factor of 20 without impairment of the time resolution.

In Publication II a scheme to stabilize the drifts of the time zero of the lifetime spectrometer is presented. An artificial reference peak is produced to serve as a basis of stabilization in a digitally stabilized multi-channel analyzer. The reference peak is created by feeding fast light pulses from a light-emitting diode along two optical fibers of different lengths onto the photomultipliers. With this system, even the fastest drifts observed in the lifetime spectrometer can be eliminated.

The shape of the annihilation line reflects the electronic structure of the annihilation site [2, 4]. Particularly, in case of vacancies decorated with impurity atoms, it contains information on their chemical identity. This information can be extracted by the so-called two-detector Doppler-broadening technique with which the background level in the spectra

can substantially be lowered [5, 6, 7, 8, 9]. In this work, a system with two high-resolution Ge detectors was taken into use. This provides the ultimate way of background reduction and improves the resolution of the system. In addition, the resolution function can be measured which enables an accurate comparison to theoretical calculations.

In semiconductors, measurements as a function of sample temperature often reveal information on the charge states of the trapping defects. The trapping rate of thermalized positrons at neutral defects is constant whereas for negative ones it is known to increase strongly with decreasing temperature [10, 11, 12, 13, 14]. The theory suggests that the positron trapping rate at negative defects would increase at least as rapidly as $T^{-0.5}$ towards low temperatures [10]. This would enable the detection of very small vacancy concentrations near zero temperature. This was one of the main motives to construct two new cryostats which enable measurements even below 10 K.

The prerequisite of strongly increasing sensitivity to negative defects is rapid positron thermalization. In Publication III, positron trapping at negative vacancy-type defects was investigated in GaAs and Si down to 8 K. The positron trapping rate in Si was observed to increase strongly even at 8 K. In GaAs, it was found that the trapping rate does not increase as rapidly as predicted for thermalized positrons below 20 K. The differences between Si and GaAs can be assigned to slower positron thermalization in GaAs than in Si. This is supported by theoretical calculations. They indicate that positron thermalization down to 10 K in heavier materials (like GaAs) may take even hundreds of picoseconds whereas in lighter hosts (like Si) thermalization may occur much faster.

In Publications IV-VI, investigations in which positron lifetime and Doppler-broadening measurements were combined to study various defects in Si and CdF_2, are described. In Publication IV, vacancies complexed with a single impurity, V-P and V-As, were identified in electron-irradiated Si. In heavily As-doped n-type Si, native vacancies decorated with three As atoms were observed. The observation of these V-As_3 centers is consistent with recent theoretical descriptions of As diffusion and electrical deactivation in highly As-doped Si [15].

In Publication V, a study of the optical properties of silicon divacancies is reported. Illumination with 0.70-1.30 eV photons was observed to affect the positron annihilation characteristics significantly. Illumination has an influence on the occupations of the different electron levels of the divacancies. The positron trapping rate again depends on the charge states of the defects. The spectral shape of the trapping rate at divacancies reveals an ionization level at 0.75 eV above the top of the valence band which is attributed to the $V^{2-/-}$ level [16].

CdF_2 is a technologically interesting material as a candidate for being used in holographic memories [17]. This application would be based on Ga and In atoms forming bistable centers in the material. Illumination with visible light and heating can be used to induce transitions of the dopant atoms between two stable positions in the lattice. The atomic structure of the bistable centers was for a long time unknown. In Publication VI, it is shown that an open-volume defect is a constituent of the deep-state atomic configuration of In and Ga in CdF_2. This is in perfect agreement with recent theoretical calculations suggesting a jump of the dopant atom from an interstitial to a substitutional site in the deep-shallow transition [18]. The results indicate that an asymmetric lattice relaxation is much more universal than previously thought, appearing from highly covalent to highly ionic compounds.

2 Positron annihilation experiments

2.1 Positrons in solids

Positron annihilation spectroscopy (PAS) is based on introducing positrons into the solid sample in which they eventually annihilate with electrons, their antiparticles [2, 3, 4]. The electronic properties of the annihilation site, which, of course, reflect the atomic structure of the lattice, leave a fingerprint in the annihilation radiation. In the annihilation, energy and momentum are conserved leading in most cases to the emission of two γ-quanta with energies of about 511 keV. There are three physical variables which contain information about the annihilation: positron lifetime, shape of the annihilation line (Doppler-broadening) and the angular distribution of the γ-quanta. In this thesis, positron-lifetime and Doppler-broadening measurements have been performed and their measurement principles are shortly described in this section.

There are two principal ways of implanting positrons in the material the choice of which depends on the depth profile under interest. When one is willing to probe the bulk properties of the lattice (in the depth of tens of micrometers), radioactive positron emitting nuclei are typically used. Positrons penetrate into the sample with a continuous energy distribution characteristic of β-decay. Therefore, the depth range at which positrons annihilate is rather wide. Investigation of thin layers again requires a controlled positron energy distribution. This is feasible by using slow-positron beams with which moderated (thermal) positrons are accelerated to a tuneable energy and a corresponding depth into the sample.

Upon entering the solid, the positron slows down quickly as a result of various electronic interactions with the host: core-electron ionization, conduction-electron scattering, etc. [19]. These processes dominate for a couple of picoseconds after which the positron mean energy is of the order of eVs. Thermal equilibrium with the material is finally achieved via phonon scattering [19, 20, 21]. At 300 K this is also rather fast in most cases, taking at the maximum some tens of ps. This is a short time compared to the positron lifetime, and therefore the nonthermal period of the positrons in the specimen is usually regarded as insignificant. However, as shown in Publication III and Sec. 3 of this overview, at low temperatures in heavy materials, thermalization may take even hundreds of ps. In such cases, the thermalization stage has an influence on the measured data and it has to be kept in mind in data analysis.

After reaching thermal equilibrium with the material, the positron diffuses around the lattice. As a thermal particle, the positron density can be described with a fully delocalized wave function. The wave function amplitude is at its highest in the interstitial volume of the lattice due to the Coulombic repulsion between the positron and the positive ion cores. Before annihilation, the positron may also get trapped at some localized level. Particularly, vacancies or larger open-volume-type defects are attractive centers to the positron due to absence of the positive nuclei. The positrons also get trapped at Rydberg levels of negative ions. The annihilation properties in a vacancy are different from those in the lattice which makes possible the identification of the defect. The intensity of the defect signal, again, is proportional to the defect concentration. Positron trapping at open-volume type defects enables positrons to be used as a point defect probe.

2.2 Positron trapping in semiconductors

In semiconductors, point defects appear in different charge states. Positrons get trapped at neutral and negative vacancies and negative ion-type centers without an open volume [10]. Positive defects repel the positron due to the long-range Coulomb interaction, and the trapping rate at them is very low compared to the annihilation rate. The trapping rate κ is proportional to the defect concentration c as $\kappa = \mu c$. The defect specific proportionality coefficient μ is called the trapping coefficient.

The trapping rate of thermalized positrons at negative defects increases strongly with decreasing temperature. This has well been demonstrated both experimentally and theoretically. The delocalized positron wave-function in the presence of a negative vacancy is a Coulomb wave. The amplitude of the Coulomb wave at the center of the vacancy increases with decreasing positron energy. This results in an increase in the overlap between the initial state and the final state wave functions, which further leads to an increase in the trapping rate. Theoretically, the trapping rate increases at least as rapidly as $T^{-0.5}$.

Negative defects induce weakly bound Rydberg states for the positron. For negative vacancies, the dominant mechanism of positron trapping at the vacancy ground state is via these Rydberg states. Since the positron binding energy at them is only of the order of tens of meVs, thermally aided detrapping can also take place at higher temperatures [22]. The overall trapping rate at negative vacancies can be written as

$$\kappa = \frac{\frac{\mu_0 c_v T^{-0.5}}{N_{\mathrm{at}}}}{1 + \frac{\mu_0 T^{-0.5}}{N_{\mathrm{at}} \eta_R} (\frac{2\pi m^* m_e k_B}{h^2})^{1.5} T^{1.5} exp(\frac{-E_b}{k_B T})}, \tag{1}$$

where $\mu_0 T^{-0.5}$ is the trapping coefficient at the Rydberg state, c_v the vacancy concentration and N_{at} the atomic density of the material. m^* represents the positron effective mass, η_R the transition rate from the Rydberg state to the ground state at the vacancy, and E_b the positron binding energy at the Rydberg state. Eq. 1 holds for thermalized positrons. As shown in Publication III of this thesis, imperfect positron thermalization at low temperatures results in a temperature dependance $T^{-\alpha}$ with $\alpha < 0.5$.

In case of neutral vacancies the positron trapping rate is constant as a function of the sample temperature. Typically, $\mu = 10^{15}$ s^{-1}. No positron trapping at positive vacancies has been observed due to the Coulombic repulsion.

2.3 Lifetime experiments

The positron annihilation rate is proportional to the overlap between the positron and electron densities as follows:

$$\lambda = \pi r_0^2 c \int d\mathbf{r} |\Psi_+(\mathbf{r})|^2 n(\mathbf{r}) \gamma[n(\mathbf{r})]. \tag{2}$$

Here, r_0 is the classical radius of the electron, c the velocity of light, Ψ_+ the positron wave function, $n(\mathbf{r})$ represents the electron density and $\gamma(n)$ is the enhancement factor of the electron density at the positron.

As mentioned above, the positron may make a number of transitions between different states during its lifetime. The annihilation rate at different positron states (denoted as λ_i) varies. In open-volume defects, the electron density seen by the positron is lower than in the ideal lattice. This results in a characteristic lifetime, $\tau_i = 1/\lambda_i$, which is longer than the lifetime in the bulk crystal, τ_B. As a rule of thumb, the vacancy lifetime is a measure of the open volume in which the positron is trapped.

The positron lifetime spectrum, i.e., the annihilation rate at time t, is the negative time derivative of the number of positrons alive at time t, $n(t)$. In practice, the measured spectrum is the convolution between the ideal spectrum and the time resolution function of the spectrometer. The ideal spectrum is always of the form

$$-\frac{\mathrm{d}n(t)}{\mathrm{d}t} = \sum_{i=1}^{N+1} I_i \lambda_i \exp[-\lambda_i t] \tag{3}$$

with the sum of relative intensities $\sum_i I_i = 1$. In a simple case where no detrapping takes place, the decay constants λ_i are directly the characteristic annihilation rates at the defects. Due to the proximity of the characteristic lifetimes in semiconductors, decompositions into more than two components are seldom possible. In a two-component analysis of a spectrum with a larger number of components, merging of components occurs.

In case of more than one positron trap, the decomposition of the spectrum often yields nonphysical results. Assuming that the fit goes through the experimental data points, the center of mass (COM) of the spectrum is, however, always a reliable parameter. It coincides with the average lifetime τ_{ave}:

$$\tau_{ave} = \int \mathrm{d}t t\Big(-\frac{\mathrm{d}n(t)}{\mathrm{d}t}\Big) = \sum_i I_i \tau_i. \tag{4}$$

If the average lifetime is longer than the lifetime in the bulk, it is an unambiguous sign of positron trapping at open-volume type defects. An interesting opportunity to analyze positron lifetime data would be to calculate the COM directly from the raw data without any fitting. In a conventional apparatus, this kind of evaluation of the τ_{ave} has not been very accurate because of drifts in the peak position. One of the aims of this thesis work was to improve the stability of the apparatus in such a way that the COM could be used as a measure of changes in the annihilation characteristics without any multiexponential fitting. The stabilization is treated in Secs. 2.3.2 and 2.3.3.

2.3.1 Conventional experimental setup

In the studies of this thesis, the positrons were obtained from a ^{22}Na source. This isotope emits positrons with a mean energy of about 300 keV. A 1275 keV $\gamma-$quantum is emitted simultaneously with the positron. This photon serves as the birth mark of the positron. The radioactive ^{22}NaCl is enclosed between thin Al-foils forming an easy-to-handle closed source. In the measurement, the source is sandwiched between two identical specimens.

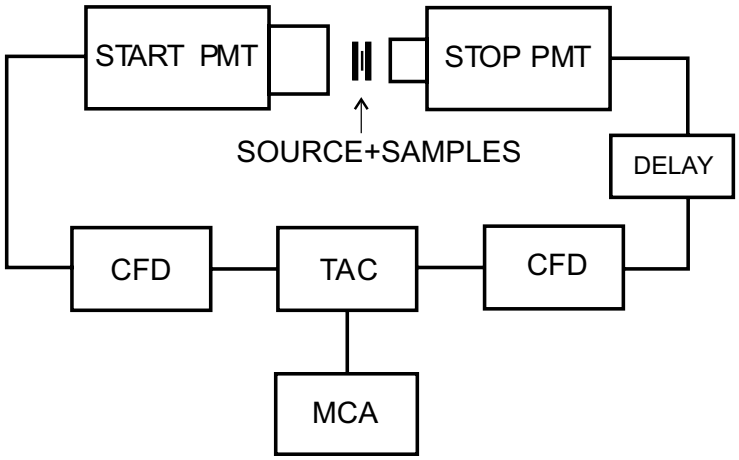

Figure 1: Conventional positron lifetime spectrometer.

In practice, the positron lifetime is measured as a time difference between two $\gamma-$quanta: the 1275-keV photon and one of the 511-keV photons released in the annihilation. The lifetime spectrum is acquired using a coincidence spectrometer with fast scintillation detectors (Fig. 1). One of the detectors is set to detect the 1275-keV γ-quantum (start-detector) and the other the annihilation γ-quantum (stop-detector). The detector pulses are fed to differential constant-fraction discriminators (CFD) which compose uniform timing signals from the detector pulses variable in amplitude. The timing signals are further led to a time-to-amplitude converter (TAC). It forms an analogue pulse whose amplitude is proportional to the time difference. Finally, the distribution of time differences is recorded with a multichannel analyzer (MCA).

The performance of a lifetime spectrometer can be quantified by its time resolution function, efficiency and stability. The time resolution and the efficiency are to some extent complementary properties; when the efficiency is increased by some means, the resolution typically worsens.

The efficiency of a scintillation detector is determined by the properties of the scintillating material and the size of the crystal. It increases with increasing mass attenuation coefficient for $\gamma-$quanta and with increasing scintillator size. The time resolution of the spectrometer arises from various parts of the apparatus. When using reasonably sized scintillators, the majority of the time spread originates from them, as a result of lengthy light production and collection times. The role of the photomultiplier tubes and the timing electronics is usually substantially smaller.

The ultimate goal of the lifetime measurement is a rapid acquisition of a spectrum from which all the physical components can be resolved. This is furthered by a narrow gaussian time resolution function, good statistics and peak-to-background ratio in the spectrum, low intensity of annihilations in the source materials and good stability of the apparatus. Usually, a good statistical accuracy is more important than an excellent time resolution [25, 26, 27].

To achieve a sufficient statistics in a reasonable time, good counting rate is desirable. It can be improved by increasing either the efficiency of the detectors or the activity of the positron source. Of these two, it is clearly wiser to enhance the efficiency. Firstly, the peak-to-background ratio is inversely proportional to the activity. The decomposibility again improves with increasing peak-to-background ratio. Secondly, the fraction of annihilations

in the source materials decreases with decreasing activity.

In this thesis, an efficient spectrometer with a sufficiently good time resolution was assembled. For this, the relation between the efficiency and the time resolution was investigated in some degree. The outcome was a spectrometer with a time resolution of 195 ps. At a face-to-face distance of 14 mm of the detectors, the counting rate is 10 cps/μCi. These figures together are very competitive with reported values [28].

Instabilities of a positron lifetime spectrometer appear e.g. as drifts of the time zero and changes in the width and form of the resolution function. These problems make the accurate analysis of the data at least difficult, if not impossible. When aiming at more accurate results by improving the statistics of the spectra, the instabilities eventually set the limits to the attainable accuracy. Therefore, enhancement of the stability is highly desirable. An example of the evident advantages would be the possibility to analyze changes in the average lifetime simply as shifts in the centroid of the spectrum. Thereby uncertainties related to multiexponential fitting could be eliminated. The measures taken in this thesis to improve the stability of the lifetime spectrometer are described in the next two sections.

2.3.2 Implementation of fast preamplifiers

An apparent problem concerning the long-term stability of the lifetime spectrometer is ageing of the PMTs. Aiming at high counting rates easily results in excessive average anode currents which lead to nonreversible degradation of the gain. Typically, a counting rate of 500 cps corresponds to an average anode current of 10–20 μA, and is known to lead to an inconvenient rate of deterioration. According to Photonis, an average current of 30 μA leads to a decrease of gain by a factor of two in about 5000 hours [29]. To achieve high stability, manufacturers recommend the average anode current to be maintained below 1 μA [29, 30, 23, 31]. With conventional apparatus and typical pulse amplitudes, this corresponds to a coincidence counting rate of the order of 50 cps which leads to very long measurement times.

The degradation of gain results in a changing pulse height distribution in the energy window. Concerning the stability of the data, this leads to changes in the resolution function and creep of the time zero of the spectrum. This is due to the nonideal amplitude-walk originating from the CFDs. In addition, the counting rate becomes lower.

In Publication I we investigated the possibility to slow down the degradation of the gain by decreasing the anode current by lowering the supply voltage over the PMT and by compensating the loss in gain by implementing fast preamplifiers at the anodes. Fast preamplifiers have been used to boost photomultiplier signals for years in various applications. In fast timing, like positron lifetime spectroscopy, the natural question that arises is whether the operating voltage over the PMTs can be decreased without impairing the time resolution of the apparatus. Typically, PMTs are driven with as high voltage as convenient, rather than a lower one. This is done because the timing properties of the PMT generally improve with increasing voltage [23, 24]. In positron lifetime spectrometers, however, the time spread related to the light production and collection in the reasonably sized scintillators is believed to be the dominating factor of the resolution. Therefore, the resolution may not necessarily worsen very rapidly with decreasing PMT voltage. Furthermore, the linearity of the PMT pulses, which is essential for the timing electronics, improves with decreasing sup-

ply voltage [29]. Hence, it is not evident what happens when the supply voltage is lowered moderately. It is, however, clear that with decreasing voltage the transit time spread of the PMT eventually diverges leading to a nonacceptable degradation of the resolution. Also, the amplifier noise may become a limiting factor with too low signal levels.

As photomultipliers we used variants of the classic XP2020 manufactured by Photonis. Plastic scintillators of size $\phi 25 \times 15\text{mm}^3$ were mounted in both detectors. Three fast preamplifiers were used: VT120A (gain 200) and VT120C (gain 20) from Ortec, and VV100B (gain 10) from LeCroy.

Concerning the timing properties of a PMT, the most essential part of the tube is the input electron optics, i.e. the region between the photocathode (pc) and the first dynode (d1) [24, 32]. We performed a series of measurements to investigate the effect of lowering the voltage U_{pc-d1} and found that to preserve the time resolution, U_{pc-d1} has to be maintained above 300 V. (Below 300 V the photoelectron collection on the first dynode degrades [33].) When lowering the supply voltage over the whole tube driven with a voltage divider recommended by the manufacturer, this condition ($U_{pc-d1} > 300$ V) does not allow a substantial decrease. Hence, we designed a new divider, with which U_{pc-d1} is 33% of the supply voltage instead of 19% with the recommended divider.

In Fig. 2, the time resolution (FWHM) of the test spectrometer as a function of the high voltage over the test tube is presented. The different markers in the figure indicate the amplification used at each point. The anode pulse amplitudes at the lower limit of the energy window have been marked in the figure. It can be seen that the time resolution is practically

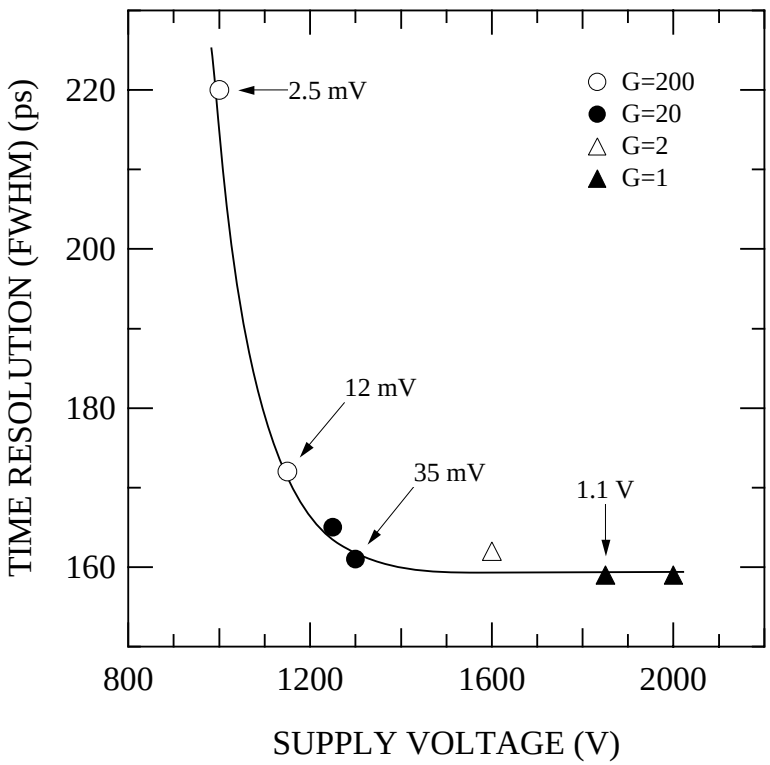

Figure 2: The time resolution of a test spectrometer as a function of the high voltage over one photomultiplier [Publ. I]. The nonamplified anode pulse amplitudes into 50 ohm are given next to the points.

independent of the high voltage in a very wide range, between 1250 V and 2000 V.

Below 1200 V the resolution worsens rapidly from the 160 ps level to a value of 220 ps at 1000 V. Besides the increase of the FWHM also the shape of the resolution function becomes distorted below 1200 V. One potential reason for the deterioration of the resolution is that the preamplifier input noise becomes important as the anode signal shrinks to millivolt level. At 1000 V the anode pulse amplitude at the lower edge of the energy window is 2500 μV which is only about 100 times larger than the rms noise amplitude at the amplifier input.

The data in Fig. 2 clearly indicate that the supply voltage of the PMTs in a spectrometer with scintillators in the cm-size range is not an important parameter. This holds on two conditions. Firstly, the voltage in the input optics of the PMT must be high enough to enable good photoelectron collection on the first dynode. Secondly, the pulse amplitudes must, of course, be high enough compared with the noise level of the amplifiers. When using the Ortec VT120C amplifier, the adequate anode pulse amplitude is some tens of millivolts. As a final test, we implemented two VT120C preamplifiers in a positron lifetime spectrometer with large scintillators and found that the quality of the data was not influenced by the preamplifiers. A three-year-long test period with the amplifiers has also shown that the rate at which the PMT gain decreases, is substantially lower than without the amplifiers.

As a conclusion, the anode pulse amplitudes and thereby the average anode current can be lowered at least by a factor of 20 without deterioration of time resolution of the apparatus. Typically, this corresponds to lowering the average anode current to the μA level at which the rate of degradation of PMT gain is known to be very low.

2.3.3 Digital stabilization based on a high-accuracy time reference

Instabilities in the lifetime spectrometer can be divided into two groups: the channel width can change (drift in gain) and the time zero can move (drift in time zero). The time zero drift can originate in all the components whereas gain changes are possible only in the TAC and the MCA. Drift in time zero means that the magnitude of the shift in channels in the MCA is independent of the time interval observed. Drift in gain, again, leads to shifts which increase with increasing time interval. To reduce the random drifts, a stabilized lifetime spectrometer was developed. The stabilization is based on an artificial time reference peak near the lifetime spectrum which a digitally stabilized MCA tries to hold in a position selected by the user. The description of the apparatus is the subject of Publication II in this thesis.

The stabilized lifetime spectrometer differs from a conventional one in two ways. Firstly, an additional apparatus creating the reference signal is needed, and secondly, the MCA is a digitally stabilized one. Ortec 919 was chosen as the MCA in this work. It is a device consisting of four different buffers, the first of which is digitally stabilized. The stabilization is based on observations of the movements of one or two reference peaks, and corresponding corrective actions. An ideal way to eliminate drifts consisting of both drift in gain and drift in time zero, would be to use two reference peaks. A peak located at the beginning of the spectrum is susceptible only to drifts in time zero and therefore serves as a good indicator of those. A peak situated at the end of the spectrum, again, is predominantly subject to drift in gain. In a modern lifetime spectrometer, the drifts are mainly time zero drifts (see Publication II). Therefore, we designed a system with one reference peak and

located it close to the lifetime spectrum. When detecting drifts in the reference peak, the MCA adjusts the offset voltage at the input amplifier of the ADC appropriately.

To stabilize drifts in all the components of the spectrometer, the reference time difference signal has to be produced at the point of light pulses entering the photomultiplier tubes. In our system, the reference peak is created by guiding light pulses from a single light-emitting diode (LED) via two optical fibers of different lengths to the photomultipliers. The transit time difference in the optical fibers is very stable and the resulting reference peak enables drifts in all components of the spectrometer to be observed and corrected. An essential design criterion of the system is, of course, that the reference peak must not move on its own, i.e. due to the instability of the apparatus creating the peak. All the shifts in its position must be fully correlated with drifts to which the real lifetime spectrum is exposed to. To achieve this, we designed a special pulser to drive the LED.

Two methods to stabilize the lifetime spectrometer have been reported in the literature [34, 35]. In both of them, the observations of the drifts are based on the lifetime spectrum itself. The accuracy of those observations is, however, not particularly good because of the low counting rate and statistics. In Publication II, it was reported that the drift rate may be very fast, even 0.5 ps in a minute. The accuracy attainable with lifetime data is of the order of 1 ps after a collection time of one minute. Hence, accurate corrections of the fastest drifts are not possible. With the LED-based system, the accuracy can be increased substantially simply by increasing the flashing frequency. With the present apparatus, the accuracy of the reference peak position after a one-minute acquisition with frequency of 6500 1/s is 0.12 ps (FWHM=210 ps). By using fast preamplifiers with gain 20, the accuracy can be enhanced to a level of 0.03 ps after a one-minute collection. This, of course, enables a much more accurate correction of the drifts appearing in a positron lifetime spectrometer.

The operation of the stabilized lifetime spectrometer described in Publication II is demonstrated in Fig. 3. There are two things to be tested in a stabilized positron lifetime spectrometer. The first is the accuracy with which the reference peak follows the real drifts of the lifetime spectrum. The second is the quality of the stabilization algorithm, i.e. how close the standard deviation of the centroids is to the theoretical minimum ($\sigma/\sqrt{N}$). Both of these properties can be studied simultaneously with the experiment described in the following.

The capability of the reference peak to detect the drifts correctly can be investigated by collecting spectra from the LED-pulser and from a ^{60}Co source at the same time. ^{60}Co emits two γ-quanta simultaneously. Thus the drifts in the centroids of the ^{60}Co spectra represent the drifts of the time zero in real positron lifetime experiments with a ^{22}Na source.

To test the performance of the digital stabilizer we record the same pulses from the TAC in two different multichannel buffers, one being stabilized and the other one not. This can conveniently be done with the Ortec Model 919 MCA consisting of four different buffers, the first of which is digitally stabilized.

Fig. 3 (a) presents the centroids of the ^{60}Co peak and the reference peak in a one-week-long measurement in the nonstabilized MCA (MCB 2). Each symbol corresponds to a 20-minute measurement. The circles represent the ^{60}Co peaks and the triangles the LED peaks. The drifts of the two peaks are identical. The overall drift of 12 ps in a week is typical for a combination of fast scintillation detectors and commercial timing electronics. The results of stabilization can be seen in Fig. 3 (b) which shows the centroids of the spectra

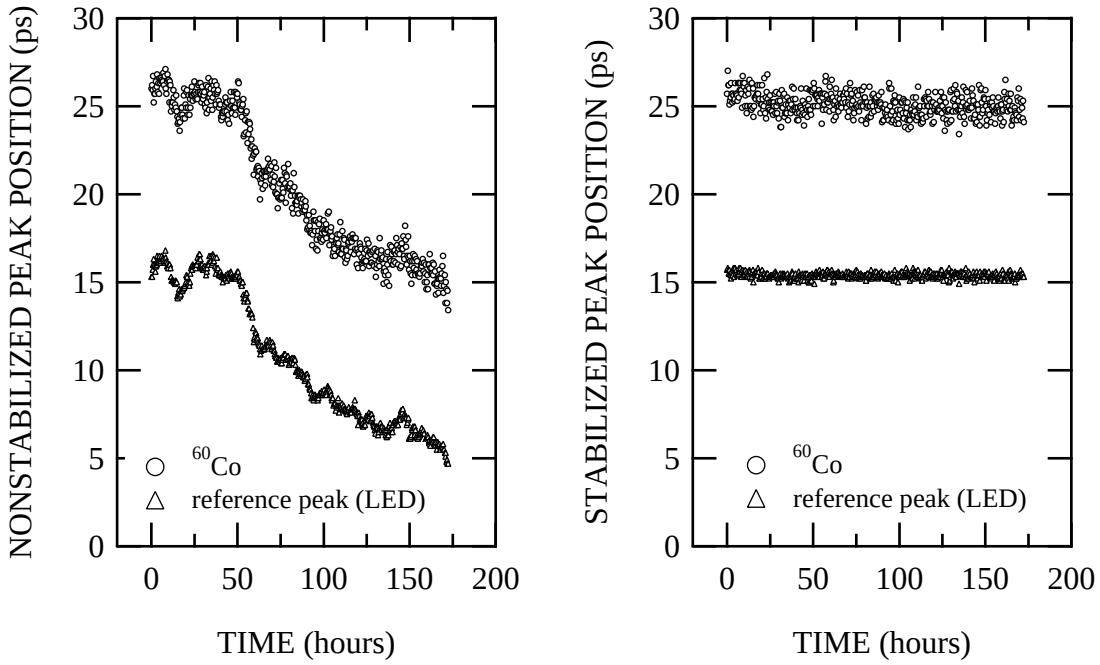

Figure 3: (a) The centroids of the reference peak and a peak resulting from the two $\gamma-$quanta from a ^{60}Co source in a one-week-long measurement [Publ. II]. As seen, the reference peak moves identically with the $\gamma-$peak and therefore properly reveals the drifts in the spectrometer. (b) The stabilized centroids of the reference peak and the ^{60}Co peak [Publ. II]. These data originate from the same pulses which lead to the data shown in (a).

collected in the digitally stabilized MCA (MCB1). As explained, these spectra originate from the same pulses as in Fig. 3 (a). The standard deviation of the reference peak centroids equals 0.17 ps whereas the theoretical STDV is about 0.03 ps. The difference probably results from the inherent delay in the correction (up to 60 s) and the rather large size of the minimum correction (0.125 ps). The centroids of the ^{60}Co spectra are within 0.6 ps (STDV) from the preset position. The theoretical standard deviation calculated from the FWHM and the number of counts is slightly lower, 0.3 ps. The residual drift in the ^{60}Co data in Fig. 3 (b) ($\leq$ 0.5 ps) can be attributed to the temperature dependence of the LED-peak position.

The results of Fig. 3 indicate that the reference peak follows well those drifts that are present in the lifetime measurement. Hence, it seems that within the accuracy achieved in this work, one reference peak located close to the lifetime spectrum is a sufficient indicator of the drifts to which the spectrum is exposed to. The data in Fig. 3 show that the apparatus presented in Publication II can be used to enhance the quality of positron lifetime data. A further improvement can evidently be attained by using software stabilization and higher reference peak frequencies.

2.4 Doppler-broadening experiments

The momentum distribution of the annihilating electron-positron pair is of the form

$$\rho(\mathbf{p}) = \frac{\pi r_0^2 c}{V} \sum_j \int d\mathbf{r} e^{-i\mathbf{p}\cdot\mathbf{r}} \Psi_+(\mathbf{r}) \Psi_j(\mathbf{r}) \sqrt{\gamma[n(\mathbf{r})]}, \tag{5}$$

where $\mathbf{p}$ is the total momentum of the annihilating pair, Ψ_+ represents the positron wave function and Ψ_j the electron wave function at state j. The distribution reflects mainly the electron momenta since the thermalized positrons are practically at rest. In the annihilation, the momentum and energy of the positron-electron pair is transferred to the pair of annihilation $\gamma-$quanta. As a result, the energies of the photons deviate from 511 keV by $\Delta E_\gamma = cp_L/2$, where c denotes the velocity of light and p_L the momentum of the positron-electron pair in the direction of $\gamma-$emission. The measurement of this Doppler broadening (DB) of the annihilation line reveals information about the distribution described by Eq. 5. In detail, the shape of the annihilation line is obtained by integrating the distribution over the directions perpendicular to the line of observation:

$$L(E_\gamma) = \int_{-\infty}^{\infty} \int_{-\infty}^{\infty} \mathrm{d}p_x \mathrm{d}p_y \rho(p_x, p_y, p_z), \tag{6}$$

$$p_z = \frac{2}{c}(E_\gamma - m_0 c^2). \tag{7}$$

A complementary way to obtain information about the momentum distribution is to investigate the deviation of the annihilation photons from collinearity. The advantage of these angular-correlation of annihilation radiation (ACAR) measurements is a considerably better resolution than achievable in DB measurements. They are plagued, however, by a notable slowness compared to DB studies.

The momentum distribution consists of the characteristic distributions of valence electrons and different core electrons. The relative intensities of the different distributions are determined by the overlap of the wave functions of positrons and each type of electrons. Annihilations with low-momentum valence electrons constitute most of the central part of the spectrum, whereas only core electrons have enough momentum to contribute to the high-momentum wings.

The core electron momentum distributions are specific to different elements. Therefore, measurement of the high-momentum region of the annihilation line may reveal the chemical identity of the atoms at the annihilation site. Comparison to theoretically calculated distributions plays an essential role in the analysis.

In vacancies, the momentum distribution is narrower than in the ideal lattice because of lower valence-electron density. In addition, the probability of an annihilation with core electrons is smaller since the positron wave function is localized further from the ion cores. Vacancies surrounded by impurities can be identified by studying the high-momentum region.

2.4.1 Conventional DB measurements

The Doppler-broadening of the annihilation line is usually measured with a high-purity Ge detector. To eliminate instabilities in the measurement electronics, digitally stabilized MCAs are routinely utilized. In the most common simple setup, only one detector is used. The energy resolution of a usual Ge detector at 511 keV is around 1.2 keV (FWHM). This is of the same order of magnitude as the Doppler broadening itself. Therefore, the measured spectrum, which is a convolution between the resolution function and the physical spectrum, is strongly influenced by the energy spread. Deconvolution of the spectrum can in principle be performed, but usually the spectra are characterized with two parameters, S and W.

The low-momentum parameter S is calculated as the fraction of counts in the central part of the annihilation line compared to the total number of counts. Typically, it is calculated in the range $|E_\gamma - 511 \text{ keV}| < 0.7$ keV. The high-momentum parameter W, again, is defined as the relative number of counts in the wing part of the spectrum, e.g. at 2.5 keV$< |E_\gamma - 511 \text{ keV}| < 4.2$ keV. The ranges at which the parameters S and W are calculated are chosen so that they measure annihilations with valence electrons and core electrons, respectively.

In a usual setup with ^{22}Na as a positron source, all the pulses observed by the Ge detector, including those arising from 1275−keV photons, are included in the spectrum. This leads to a rather poor peak-to-background ratio of about 200. This means that the high-momentum part of the spectrum is distorted by background events already at 15 mrad (4 keV). Therefore, conventional single-detector measurements are not very well suited for identification of the chemical nature of the annihilation sites. The techniques to reduce the background are treated in the following.

2.4.2 Two-detector DB measurements

The background of the Doppler-broadening spectrum measured with a single detector consists of various undesired events. First, pulses originating from the nuclear γ-quanta or other high-energy photons via Compton-scattering are observed in the energy range of the annihilation photons. Second, pulses from different simultaneous photons may be piled up leading to a background event. Additionally, the spectrum gets distorted on the low-energy side due to incomplete charge collection in the detector.

The ultimate background reduction can be realized by requiring that both annihilation photons emitted collinearly are detected simultaneously, and that the observed sum energy equals to $2m_0c^2 - E_b$. Here, m_0c^2 is the rest energy of the positron and the electron, and E_b the binding energy of the positron and the electron in the solid.

A simple and inexpensive way of reducing the background in the high-energy side is to use a NaI detector (or equivalent) collinearly with the Ge detector to observe the other annihilation photon [6]. With this technique the peak-to-background ratio can be improved to $10 - 20,000$ [5]. This corresponds to extending the background-free momentum region up to 40 mrad. Due to the rather poor energy resolution of the typical NaI detectors, the energy-conservation rule cannot be exploited. Therefore, some residual pile-up events are inevitably accepted in the recorded Ge-detector spectrum. This distorts the high-momentum region of the spectrum leading to problems in the analysis of the data. Some numerical pile-

up reduction algorithm can be used but they are unavoidably approximative. However, core-electron momentum spectroscopy using the two-detector coincidence measurements has been succesful in the identification of various defects in semiconductors.

The best practical approach towards the ideal background-reduction scheme presented above is to use two collinearly set Ge detectors and a multiparameter analyzer (MPA) [7, 8, 9]. The MPA records the detector pulses in a two-dimensional map thereby retaining the information on the energies of both annihilation photons. The electron-momentum spectrum is resolved from the raw data as $p_z = (E_1 - E_2)/c$ where E_1 and E_2 are the energies of the individual photons. With this system, the peak-to-background ratio is enhanced up to $2,000,000$. This is simply based on the fact that since the resolution of both detectors is good, wrong events can be ruled out efficiently by the requirement of energy conservation. With two Ge detectors, the utilizable momentum range extends even up to 70-80 mrad.

A further advantage of the Ge-Ge system is an improvement of the energy resolution. Since the experimental signal for the momentum is twice that obtained with a single detector, but the uncertainty increases only quadratically, the energy resolution of the instrument is better by a factor of $\sqrt{2}$. With usual Ge detectors this corresponds to an improvement from 1.2 to 0.9 keV (FWHM). The resolution function of the system is obtained as a by-product of the measurement. It is the distribution of the counts as a function of $E_1 + E_2$. Since the resolution function is accurately known, comparison of the electron-momentum distributions with theoretical distributions is on a sound basis.

Due to the efficient reduction of pile-up pulses, data acquired with the Ge-Ge system can be used as a reference for composing the numerical pile-up-reduction algorithms for spectra collected with NaI-Ge systems. Fig. 4 shows the momentum-distribution measured in (100)-Si with both two-detector systems. A single exponential function has been subtracted from the raw data of the NaI-Ge system such that the data in the high-momentum regions are identical. This same functional form can then be used for other measurements in Si with the NaI-Ge apparatus. The difference in the resolution of the systems can be seen in the low-momentum part of the spectrum. In the course of this thesis work, a two-Ge-detector Doppler-broadening apparatus was taken into use for the defect studies in Laboratory of Physics. In the investigations presented in Publication IV, it was utilized to obtain the correct pile-up-reduction for the data actually measured with a NaI-Ge coincidence system.

2.5 Sample treatment

Variation of the sample temperature is most useful in the investigations of point defects in semiconductors since, for instance, the states of the defects often depend strongly on it. From the point of view of positron spectroscopy, measurements as a function of the temperature may reveal the charge state of the positron traps. During this thesis work, two cryostats based on closed-cycle He-cryocoolers have been constructed, one operating in the range 6.5-350 K and the other in 12-350 K. All the measurements presented in publications III-VI were done with these apparatuses.

Illumination of the specimen is another way of varying the occupations of the defect levels. In our setups, monochromatic light is obtained from a halogen lamp via a monochromator. The sample sandwich is illuminated on both sides using a trifurcated optical fiber. One of the branches of the fiber is for the photon flux monitoring with a Si/Ge detector.

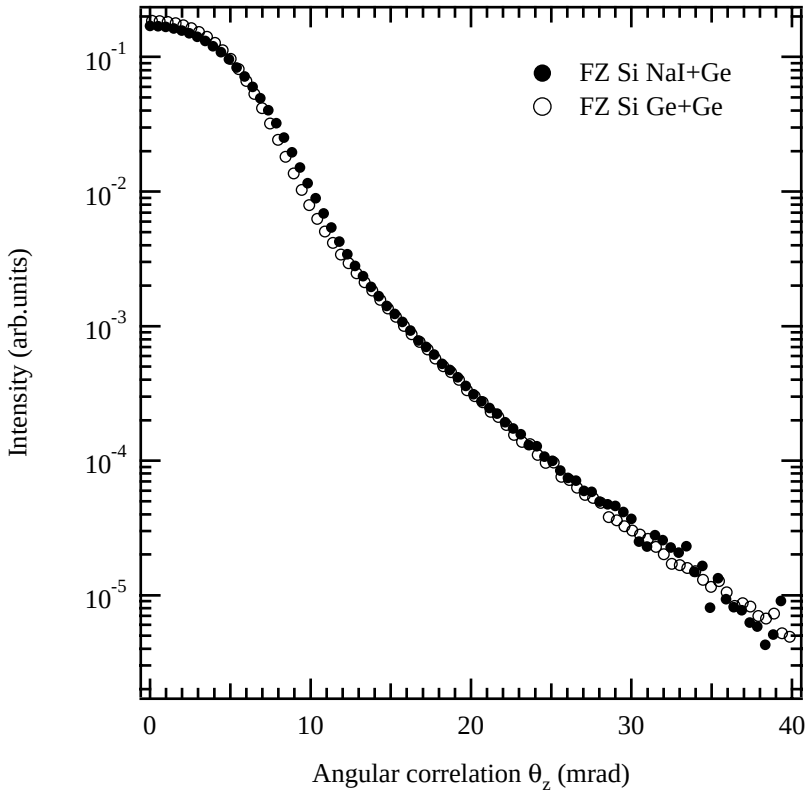

Figure 4: The electron-momentum distribution in (100)-Si measured with NaI-Ge and Ge-Ge coincidence techniques.

The photon-energy range in our system is $h\nu = 0.6 - 3.0$ eV and the photon-flux range $\phi = 10^{12} - 10^{16}$ cm^{-2} s^{-1}.

The sample treatment as well as the positron measurements are fully automated under the control of a personal computer (program Datcd) [36].

3 Positron thermalization in Si and GaAs

Positron thermalization in solids is generally believed to occur quickly compared to the positron lifetime in the lattice [4]. ACAR-measurements performed in simple metals suggest that the positron is in thermal equilibrium with the host at the time of annihilation even at 10 K [37]. Even neutral positronium atoms were found to thermalize to 10 K in quartz within the average lifetime of 125 ps [38]. The rapidity of thermalization is supported by theoretical calculations in aluminum [21]. Both experiments and calculations indicate that when considering low temperatures, phonon scattering is the dominating energy-loss mechanism [19, 20, 21, 38].

Generally, the rapidity of thermalization has been accepted to be true irrespective of the material. However, from the classical point of view, positron-phonon scattering in a heavy material could be expected to be less efficient than in a light host. In Publication III, this side of the thermalization problem is addressed with both calculations and a new experimental approach.

3.1 Experiments

ACAR experiments probe the positron momentum distribution at the time of annihilation. A more sensitive way to investigate thermalization could be the measurement of the temperature dependence of positron trapping rate at negative vacancies. Namely, it measures the positron energy distribution at the time when the positron escapes from the delocalized state either by annihilation or trapping. This time is, of course, earlier than annihilation. The sensitivity to positron energy comes from the energy-dependent trapping rate.

The positron trapping rate at negative vacancies is known to increase strongly towards low temperatures [10, 11, 12, 13, 14]. For fully thermalized positrons, the theory predicts a dependence of $\mathrm{T}^{-\alpha}$ with $\alpha \geq 0.5$ [10]. The increase results from the enhancement of the delocalized positron wave function at the vacancy with decreasing positron energy. This again leads to the increase of the overlap between the delocalized state wave function and the wave function at the vacancy ground state, and thus to an increasing trapping rate at the vacancy. For a positron with an energy E, the trapping rate is proportional to $1/\sqrt{E}$.

If the positron thermalization is incomplete or slow, the positron energy does not attain the equilibrium distribution soon enough after the implantation. The effective trapping rate thus cannot increase as rapidly as in the ideal situation. If it is observed to increase with decreasing host temperature according to $T^{-\alpha}$ with $\alpha < 0.5$, this can be attributed to incomplete thermalization.

Positron trapping at negative vacancies in GaAs was studied in a commercial undoped sample. In darkness, negative Ga vacancies act as the only positron traps. The lifetime spectra were decomposed with a second component of 260 ps in agreement with earlier investigations. The average lifetime at 300 K is 231 ps, and it increases rapidly down to 25 K, reaching a value of 239 ps. In Fig. 5, the average positron lifetime is presented from 8 to 50 K. From 50 to 25 K it increases about 2 ps, but from 25 to 8 K, at the most, 1 ps.

From previous studies, it is known that the model described by Eq. (1) in Sect. 2.2 is very well compatible with the positron trapping data related to the V_{Ga} from 300 K down

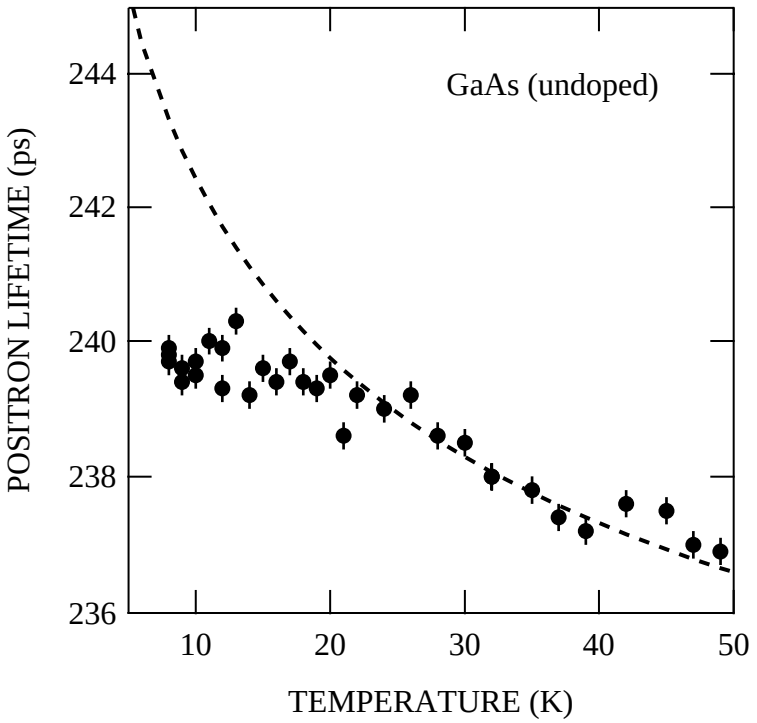

Figure 5: The average positron lifetime vs sample temperature in undoped GaAs [Publ. III]. The dashed line shows the lowest lifetimes explainable by the theory which assumes the positrons to thermalize instantly after the implantation.

to about 30 K[2, 11]. When trying to extend the fit to lower temperatures with the present data (Fig. 5), we find that the best fit follows the data nicely down to 20 K below which the fit gradually rises above the data. This is seen in Fig. 5 in which the dashed line represents the best fit. This fact is qualitatively in agreement with the idea that imperfect positron thermalization plays a role at low temperatures.

In electron-irradiated pure Si, in a sample containing negative divacancies, we observed that the positron lifetime increases strongly from 20 to 8 K (see Publication III, Fig. 4). This can be interpreted as an evidence on rapid positron thermalization in Si. Our experimental data in GaAs and Si indicate that positron thermalization in Si is faster than in GaAs. To lay the experimental observations and interpretations on a stronger basis, we performed theoretical calculations on positron thermalization in Si and GaAs.

3.2 Theoretical calculations

The time evolution of the positron momentum distribution is given by the Boltzmann equation [21, 39]. The rate of change in the occupation $n(\mathbf{q}, t)$ of momentum state $\mathbf{q}$ is calculated as the difference between the rate at which positrons from all other states make transitions to the state $\mathbf{q}$, and the rate at which positrons at state $\mathbf{q}$ make transitions to all the other possible states. In a homogenous medium the Boltzmann equation reads:

$$\frac{d}{dt}n(\mathbf{q},t) = \int d^3q'[W(\mathbf{q}',\mathbf{q})n(\mathbf{q}',t) - W(\mathbf{q},\mathbf{q}')n(\mathbf{q},t)] - [\lambda + \kappa(\mathbf{q})]n(\mathbf{q},t) + n_{\mathrm{init}}(\mathbf{q},t). \quad (8)$$

Here $n(\mathbf{q},t)d^3qdt$ is the probability of finding the positron in a momentum element $\hbar^3 d^3q$ around $\hbar\mathbf{q}$ within time interval $[t, t+dt]$. $W(\mathbf{q},\mathbf{q}')d^3q'$ is the transition rate from momentum $\hbar\mathbf{q}$ to momenta in the volume d^3q' at $\hbar\mathbf{q}'$, which is to be calculated with Fermi Golden Rule. Further, λ denotes the annihilation rate in the delocalized state, $\kappa(\mathbf{q})$ the momentum dependent trapping rate, and $n_{\mathrm{init}}(\mathbf{q},t)$ represents the initial positron source.

In semiconductors, the role of positron-electron scattering in the thermalization to low temperatures is negligible due to the band-gap. In addition, in Si and GaAs, all the other types of phonons except longitudinal-acoustic phonons play a minor role when considering thermalization to temperatures below 100 K [40, 41]. Hence, in our calculations, we only took into account positron scattering off longitudinal-acoustic phonons. The scattering rate can be expressed as:

$$\begin{aligned} W_{\mathrm{ph}}(\mathbf{q}',\mathbf{q}) &= \frac{\gamma^2}{4\pi^2}k\{[f_B(\hbar c_s k)+1]\delta(E_+(\mathbf{q}')-E_+(\mathbf{q})-\hbar c_s k)\delta_{\mathbf{q}',\mathbf{q}+\mathbf{k}}\Theta(\omega_D - c_s k) \\ &\quad + f_B(\hbar c_s k)\delta(E_+(\mathbf{q}')-E_+(\mathbf{q})+\hbar c_s k)\delta_{\mathbf{q}',\mathbf{q}-\mathbf{k}}\Theta(\omega_D - c_s k)\}. \end{aligned} \tag{9}$$

Here we use the Debye approximation for the phonon dispersion relation, $\omega = c_s k$, where c_s is the velocity of the acoustic waves in the material and k the length of the phonon wave vector $\mathbf{k}$. ω_D denotes the Debye cut-off frequency which is calculated from the Debye temperature Θ_D as $\omega_D = k_B\Theta_D/\hbar$. In the deformation-potential approximation the square of the positron-phonon coupling constant is $\gamma^2 = E_{\mathrm{def}}^2/2NMc_s$. N is the ion density and M the ion mass, $f_B(E)$ denotes the Bose-Einstein distribution ($f_B(E) = [exp(E/k_BT)-1]^{-1}$) and $E_+(\mathbf{q}) = \hbar^2q^2/2m^*$ the energy of a positron with an effective mass m^*.

A FORTRAN program code was written to solve the Boltzmann equation numerically. The results for Si and GaAs are illustrated in Fig. 6. The curves present the times that are required by the positrons to reach the mean energies of $2\times E_{\mathrm{th}}$ and $1.1\times E_{\mathrm{th}}$. After reaching the latter energy, the positrons appear as fully thermalized particles from the experimental point of view. In Si, thermalization even down to 10 K seems to be rather fast: positrons get within 10 % of the final thermal energy in 70 ps. Below 10 K, complete thermalization, however, takes a time which is comparable to the mean lifetime in the lattice ($\tau_{\mathrm{Si}} = 218$ ps). In GaAs, thermalization times are considerably longer than in Si at all temperatures. At 10 K it takes about 80 ps for the positrons to reach a mean energy of $2\times E_{\mathrm{th}}$, and about 180 ps for $1.1\times E_{\mathrm{th}}$. At 4 K it takes nearly 400 ps for the thermalization within 10 % of the sample temperature.

The calculations indicate that depending on the temperature (4–100 K), the thermalization times in GaAs are 2–4 times longer than in Si. A more careful investigation points out that the difference is mainly due to the difference in the mass densities ρ of the materials (see Publication III). The scattering rate is inversely proportional to the mass density, and since the ratio $\rho_{\mathrm{GaAs}}/\rho_{\mathrm{Si}} = 2.5$, the mass density can be regarded as the main reason for the difference.

The main question is, of course, if the results of the calculations can explain the experimental data at low temperatures. The effect of incomplete thermalization on the positron trapping properties can be evaluated by calculating a time-dependent trapping rate $\kappa(t)$ from the theoretical positron-mean-energy data. The calculations indicate that the positron momentum distribution during thermalization is close to a MB distribution at all stages. Then,

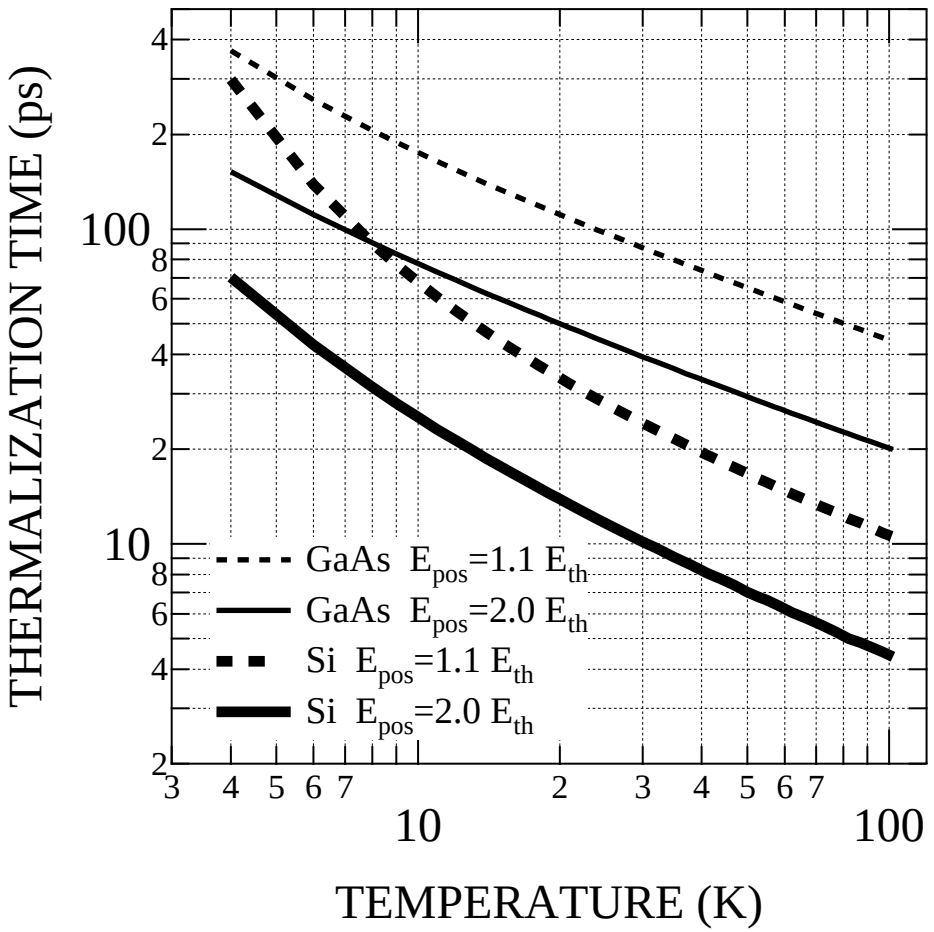

Figure 6: The positron thermalization time vs sample temperature in Si and GaAs [Publ. III]. The solid curves indicate the time needed for the positrons to reach the mean energy equalling twice the thermal energy. The dashed lines again represent the level of $1.1 \times E_{\mathrm{th}}$.

the trapping rate $\kappa(t)$ is proportional to $\bar{E}(t)^{-0.5}$. From $\kappa(t)$ one can proceed to calculate the trapping fraction which can be directly compared to the experimental results. Fig. 7 presents the experimental data with circles. The solid line, again, shows the best fit which takes the calculated $\bar{E}(t)$ into account. As can be seen, the agreement is rather good over the whole temperature range. To illustrate the effect of imperfect thermalization on the trapping fraction, the dashed line shows how the trapping fraction would behave if the positrons were thermal at the time of implantation. The same defect-related parameters were used with both lines, and therefore the difference stems purely from the different thermalization.

Due to the complicated nature of our experimental Si data, a similar comparison was not attempted. Nevertheless, the lifetime data obtained in the Si samples support the calculations predicting faster thermalization in Si compared to GaAs.

As a conclusion, the experiments and calculations indicate that positron thermalization to low temperatures, like 10 K, may take a considerable time compared to the lifetime in the lattice. The mass density of the material plays an essential role in the thermalization process via acoustic-phonon scattering. In heavy materials, positron thermalization takes a longer time than in lighter hosts. As a consequence of the possible slow thermalization, some care should be taken when interpreting experimental positron data at the lowest temperatures.

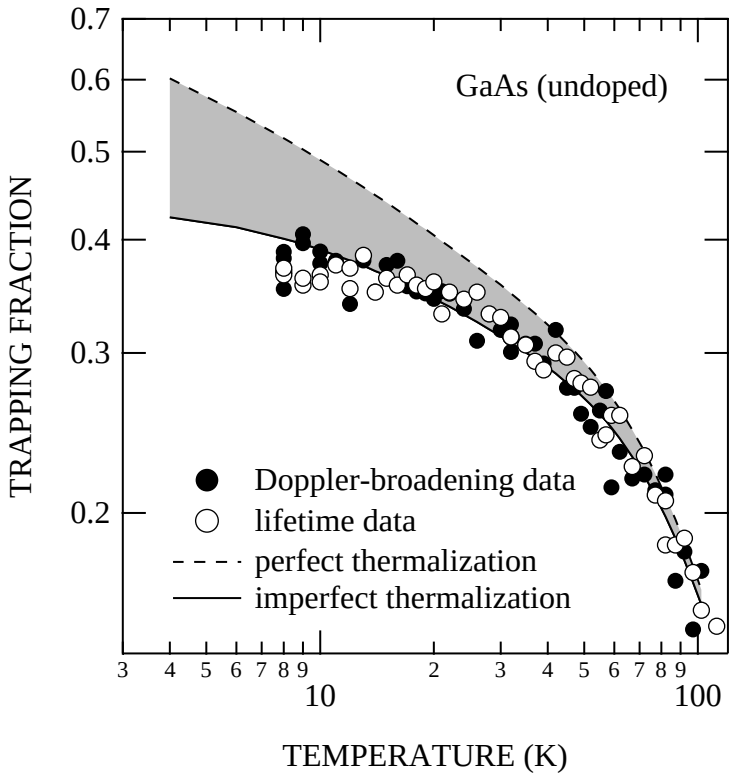

Figure 7: The positron trapping fraction at Ga vacancies in undoped GaAs as a function of sample temperature [Publ. III]. The solid line describes the best fit with the model which takes the calculated thermalization behavior into account. If the positrons are assumed to be thermal at the time of implantation, but the same defect-related parameters are used as with the solid-line fit, the temperature dependence of the trapping fraction is that shown by the dashed line. The shading illustrates the effect of imperfect positron thermalization in GaAs.

4 Applications to semiconductors

4.1 Vacancy-impurity complexes in Si

In the As and Sb doping of Si the concentration of free electrons saturates at the level $\leq 5 \times 10^{20}$ cm^{-3} when the impurity concentration is increased [1]. This is indicative of the formation of inactive impurity clusters or compensating defects that trap free electrons. Experimental evidence on various defects has been obtained in heavily doped Si. Dopant precipitates and different $V_n d_m$ complexes have been observed [15, 42, 43]. There is, however, no consensus on the structure of the dominating deactivating defects. To gain insight into this question, we investigated several Czochralski-grown Si samples doped with P and As. Doppler-broadening measurements aided by lifetime studies were performed.

We studied Czochralski-grown (CZ) Si(111) bulk crystals doped with As ([As]=10^{19} and 10^{20} cm^{-3}) and P ([P]=10^{20} cm^{-3}). Experiments were done in as-grown samples as well as after electron irradiation with 2-MeV electrons at 300 K. Investigations with other techniques have indicated that electron-irradiated samples contain V-As and V-P pairs [44]. These irradiated samples thus provide us a possibility to measure the positron annihilation characteristics of the simple complexes.

The lifetime measurements show that there are no vacancies trapping positrons in the as-grown samples Si([As]=10^{19} cm^{-3}) and Si([P]=10^{20} cm^{-3}). In the heavily As-doped sample ([As]=10^{20} cm^{-3}), the average lifetime at 300 K is 232 ps. This is clearly higher than the lifetime in the lattice (220 ps) indicating the presence of vacancy-type defects. The spectrum has two components with $\tau_2 = 250 \pm 3$ ps. This is the characteristic positron lifetime at a monovacancy in Si.

In all electron-irradiated samples the average positron lifetime is longer than in as-grown samples, indicating that irradiation-induced vacancies are observed. The average lifetime is also independent of the irradiation fluence which can be attributed to saturation trapping. The lifetime values 247 ± 2 ps show that the vacancies are monovacancies.

To identify the monovacancies in more detail, Doppler-broadening spectra were recorded using the two-detector coincidence technique. In case of one type of a vacancy, the spectrum is of the form $\rho(p) = (1-\eta)\rho_B(p) + \eta\rho_V(p)$, where $\rho_B(p)$ and $\rho_V(p)$ are the momentum distributions in the lattice and at the vacancy, respectively. η is the fraction of positrons annihilating in the monovacancy. Since the momentum distribution in the lattice $\rho_B(p)$ can be measured in the reference sample, and the trapping fraction η can be calculated from the lifetime data, the distributions $\rho_V(p)$ can be resolved from the measured spectrum $\rho(p)$. They are shown in Fig. 8 for the monovacancies observed in as-grown Si([As]=10^{20} cm^{-3}) as well as in irradiated Si([As]=10^{20} cm^{-3}) and Si([P]=10^{20} cm^{-3}).

The momentum distributions $\rho(p)$ at vacancies indicate large differences in the higher momenta ($p > 12 \times 10^{-3} m_0 c$), where annihilations with core electrons contribute most (Fig. 8). Since the core electron momentum distribution is characteristic for a given atom, the differences between the spectra in Fig. 8 indicate different atomic environments of the vacancy in each of the three cases. Because in both Si (Z=14) and P (Z=15) the $2p$ electrons constitute the outermost core electron shell, the core electron momentum distributions of these elements are very similar. The crucial difference in the core electron structures of Si, P, and As is the presence of $3d$ electrons in As. The overlap of positrons with the As $3d$ electrons

is much stronger than with the more localized Si or P $2p$ electrons. The large intensity of the core electron momentum distribution is thus a clear sign of As atoms surrounding the vacancy.

In the electron-irradiated samples all the positrons annihilate at vacancies according to the lifetime measurements. Since the irradiation is known to produce V-P and V-As complexes in P and As doped Si, respectively, the core electron momentum distributions can be attributed to these defects. The influence of As next to the vacancy is clearly visible as an enhanced intensity in the high-momentum region. Since an even stronger signal from As is seen in the as-grown Si([As]=10^{20} cm^{-3}), we can conclude that this monovacancy is surrounded by at least two As atoms. Quantitative analysis on the number of As atoms can be done by calculating the conventional W parameter in the momentum range $20 \times 10^{-3} < p/m_0c < 25 \times 10^{-3}$. Because of the similar core electron structure of Si and P, the value $W_V/W_B = 0.71$ measured for the V-P pair is expected to be close to that of an isolated monovacancy. The value W_V/W_B increases by 0.28 to 0.99 ± 0.03 in the V-As complex as a result of $3d$ electron annihilations of a single As atom. In Si([As]=10^{20} cm^{-3}), $W_V/W_B = 1.49$, corresponding to an increase of 0.78. This is exactly three times the contribution of a single As atom suggesting that the dominating defect in the as-grown sample is V-As$_3$ complex.

To put the above experimental interpretations on a firmer basis, theoretical *ab initio* calculations were performed for both the positron lifetime and momentum distributions. The

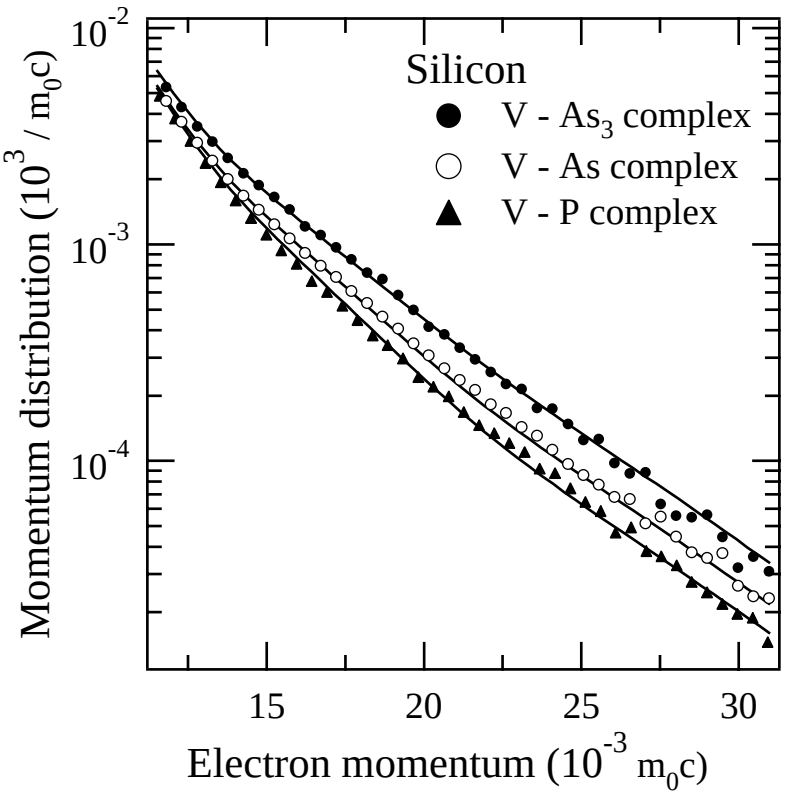

Figure 8: The high-momentum part of the positron-electron momentum distribution at the various vacancy-impurity pairs, identified in electron-irradiated Si([P]=10^{20} cm^{-3}), and in as-grown and irradiated Si([As]=10^{20} cm^{-3}) [Publ. IV]. The results of theoretical calculations are shown by the solid lines.

lifetime values for monovacancies decorated with P and As atoms are in very good agreement with the experimentally observed lifetimes. The calculated core-electron momentum distributions for V-As, V-P and V-As_3 are shown in Fig. 8. As seen, the agreement is excellent. Also the valence-electron part of the distribution reproduces the experimental curve very well. The calculated distributions for $V - As_2$ and $V - As_4$ are in strong disagreement with the observations. Thus, supported by the theoretical calculations, we identify V-As_3 in as-grown Si([As]=10^{20} cm^{-3}). This defect may play a role in the electrical deactivation in highly As-doped Si.

4.2 Optical properties of the divacancy in Si

Point defects in semiconductors possess localized electron states in the band gap. The occupation of these levels can be controlled by, e.g., photoexcitation. This technique has been used extensively to study the properties of point defects with various spectroscopies. Positron annihilation accompanied with photoexcitation has been utilized to study, for instance, As vacancies in GaAs [45]. In Publication V of this thesis, we investigate the optical properties of divacancies in Si.

A controlled way of introducing divacancies in Si is electron-irradiation at room temperature [44]. Together with divacancies, also vacancy-impurity complexes are formed. Their contribution to the positron signal can in many cases, however, be distinguished by combining positron-lifetime and Doppler-broadening measurements.

Four samples were irradiated at room temperature with 2-MeV electrons. One of them (F1) was p-type undoped FZ Si which was irradiated to a fluence of 1×10^{18} e$^-$/cm^{-2}. Three others (C1, C2 and C3) were of p-type CZ material and were subjected to fluences of 3×10^{17}, 1×10^{18} and 5×10^{18} e$^-$/cm^{-2}, respectively. After the irradiation, divacancies and vacancy-oxygen pairs (A-centers) were observed by combining positron-lifetime and Doppler-broadening measurements as a function of temperature.

The positron results were found to be strongly influenced by illumination with (0.70–1.30 eV) photons. The average positron lifetime measured under illumination exhibits changes of about 15 ps with the values around the levels measured in darkness. The combination of lifetime and DB-results indicates that the light-induced changes can be fully attributed to changes in the positron trapping rate at the divacancies, not at the V–O pairs.

Fig. 9 shows the positron trapping rate κ_{V_2} at the divacancies measured under illumination at 15 K as a function of the photon energy. The trapping rates in darkness are also shown in the figure with dotted lines. Under illumination with photons of $0.70 - 0.75$ eV energies, the trapping rate is lower than in darkness in all CZ-grown samples. The difference between κ_{V_2} in the dark and under illumination is the larger the higher the irradiation fluence had been. In all samples, the trapping rate increases strongly above 0.75 eV and levels off at about 0.90 eV. The shape of the curve between 0.70 and 0.90 eV is similar in each sample. Above 1.0 eV, κ_{V_2} decreases in all samples in a way which seems to depend on the sample.

With divacancies in different charge states q, the total trapping rate κ_{V_2} equals $\kappa_{V_2} = \sum_q \mu_{V_2^q}[V^q]$. The changes in κ_{V_2} demonstrate that the occupation of the different charge states of the divacancies depends on the photon energy. The photon flux in the measurements described in Fig. 9 is 1×10^{16} cm^{-2} s^{-1}. This flux was observed to be high enough such that the occupations of the different electron levels of the divacancies are fully determined by

the electron and hole emission cross sections from different electron levels of the divacancies. Carrier capture rates do not play any role (for the discussion, see Publication V). This means that the occupation of different levels is the same for all samples irrespective of the irradiation fluence.

EPR measurements reveal three ionization levels of the divacancy in the band gap [16]. The acceptor level $V_2^{2-/-}$ is located at $E_c - 0.40$ eV and the donor level $V_2^{0/+}$ at $E_v + 0.23$ eV, where E_c and E_v are the energies at the bottom of the conduction band and at the top of the valence band, respectively. The $V_2^{-/0}$ level is between these two, probably near the midgap. The photon-energy dependence of the positron trapping rate κ_{V_2} under illumination is in agreement with this level scheme as explained in the following.

In darkness, the Fermi level is located at about midgap. Part of the divacancies are in the neutral and part in the singly negative charge state. EPR measurements show that the $V^{-/0}$ level gets filled with increasing irradiation fluence [16]. Below 0.75 eV photon energies, the only possible transitions are electron excitation from the valence band to the $V^{-/0}$ level, and from this level up to the conduction band. The decrease in the trapping rate shows that the $V^{-/0}$ becomes less occupied under illumination. The fact that the decrease in κ_{V_2} is larger for the more heavily irradiated samples is understandable based on the EPR observations.

The rapid increase in κ_{V_2} above 0.75 eV can be ascribed to the onset of electron excitations from the valence band to the double acceptor level $V^{2-/-}$. With these transitions the divacancies become more negative leading to an increase in κ_{V_2}.

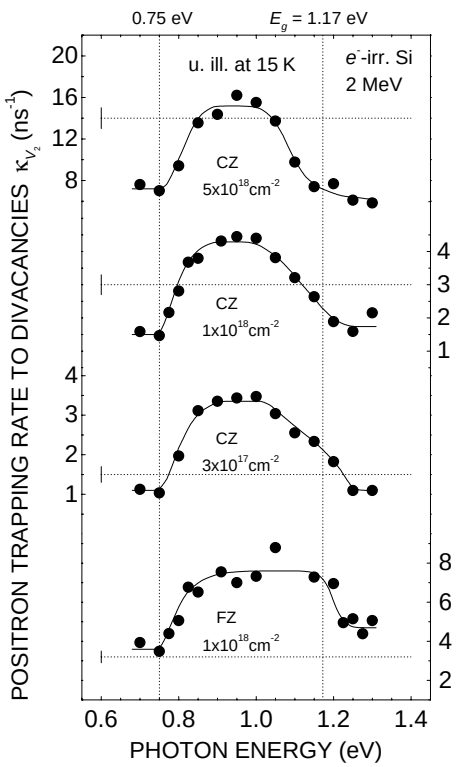

Figure 9: Positron trapping rate κ_{V_2} to divacancies in electron-irradiated FZ Si (sample F1) and CZ Si (samples C1-C3) at 15 K under illumination with monochromatic light [Publ. V]. The dotted horizontal lines indicate the values of κ_{V_2} in darkness at 15 K. The solid lines are guides to the eye.

4.3 Bistable centers in CdF_2

Bistable centers are some of the most fascinating point defects appearing in semiconductors. The charge carriers are captured at these either on localized orbits or in effective mass bound states. The purpose of of the studies presented in Publication VI was to investigate if positron annihilation spectroscopy can produce new information on the structure of the bistable centers in CdF_2. Positron lifetime and Doppler-broadening measurements in four different CdF_2 samples are reported. One In-doped sample and two Ga-doped ones were known to contain bistable centers. An Y-doped sample was used as a reference since Y is a simple effective-mass donor in CdF_2 [46].

Positron measurements in darkness reveal the existence of some native vacancies and negative ions. Combining the results with theoretical formation energy calculations [47] let us infer that these defects are most probably Cd-vacancies and F-interstitials.

The key experiment concerning defect bistability is to study whether illumination has an influence upon positron trapping. Illumination is known to induce deep-shallow transition of the bistable centers. A most pronounced effect is observed in both In and Ga doped crystals at 15K: the mean positron lifetime decreases with increasing photon fluence and saturates to a value of 1-4 ps lower than obtained before illumination. The changes are persistent at 15 K: after an illumination the average lifetime remains constant for days. In contrast to these effects, the illumination has no influence on the positron lifetime in the Y doped sample.

To study the thermal stability of the observed persistent change in the average lifetime we performed an isochronal annealing experiment (Fig. 10). The samples were first illuminated with 1.95 eV (In-doped) or 3.0 eV (Ga-doped) photons whereafter the measurements and the heat treatments were performed in the dark. In In-doped CdF_2, annealing in the range from 60 K to 75 K restores the lifetime at the initial level before illumination. In case of the Ga doped CdF_2, the recovery occurs between 200 K and 250 K. These temperatures are the same at which the bistable centers make the transition from the shallow state to the deep state [46].

We also investigated the correlation between the optical absorption properties and the positron lifetime. In the experiment, we illuminated the samples to a constant fluence with variable photon energies and measured the positron lifetime in darkness after each illumination. With increasing photon energy, the lifetime and the optical absorption start to increase at the same energy. This data together with that presented in Fig. 10 show that the average lifetime is sensitive to the state of the bistable centers. Positron trapping at open-volume defects is enhanced, i.e. more vacancies are detected, when the deep state is occupied.

Combining the results of positron lifetime and Doppler-broadening measurements reveals that there are two different types of vacancies in the samples, the Cd-vacancies and some others. The latter ones cease to trap positrons when In and Ga are converted to the shallow state by illumination. We can thus deduce that the vacancy defect is a constituent of the deep state atomic structure of the bistable centers in CdF_2. This conclusion is supported quantitatively by the concentration estimates obtained from the positron results which are of the same order of magnitude as those from electrical and optical measurements.

By comparing the lifetime results and theoretical lifetime calculations one can further infer that the size of the open volume related to the deep state is at least half of a Cd-

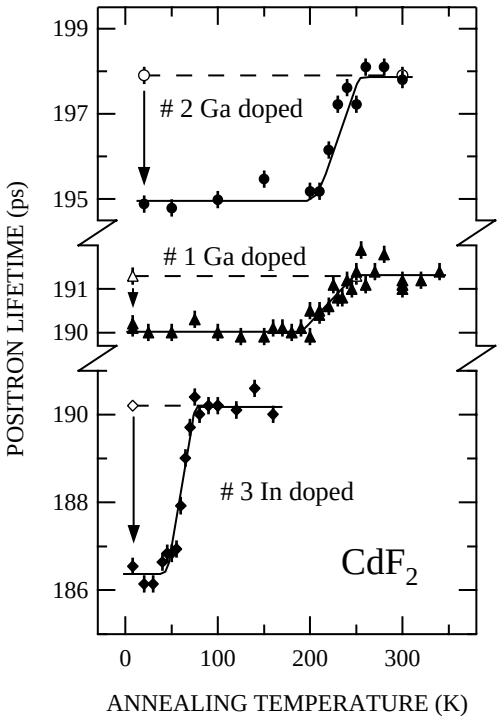

Figure 10: The average positron lifetime measured at 15 K in darkness as a function of the annealing temperature [Publ. VI]. Before each 10 min annealing the samples were illuminated at 15 K with 1.95 eV (In-doped) or 3.0 eV (Ga-doped) light. The illumination was long enough to saturate the change in the average positron lifetime (photon fluence 2×10^{17} cm^{-2}). The open symbols and the dashed lines represent the lifetime levels before illumination. The solid lines are guides to the eye.

monovacancy.

Most excitingly, the positron annihilation results on the DX center in $Al_xGa_{1-x}As$ [2, 48] are qualitatively very similar to those in CdF_2. In $Al_xGa_{1-x}As$, the donor atom is believed to make a substitutional-interstitial jump leaving an open volume behind which positrons detect [2, 48]. In the transition the sp^3-type bonding changes to a sp^2-type one. Very recent calculations by Park and Chadi [18] suggest that also in CdF_2 In and Ga atoms can move from the substitutional site to an interstitial site in the neighbouring lattice cell. The donor atom is stabilized to the interstitial site as a result of hybridization of the d-electrons of the donor and Cd-atoms. This model is fully compatible with our positron data. As a conclusion, our positron results imply that the bond-breaking mechanism resulting in asymmetric lattice relaxations is of much more general validity than previously thought; it applies from covalent to predominantly ionic systems.

5 Summary

In this thesis, instrumentation and methods for positron annihilation spectroscopy of defects in semiconductors have been developed. In addition, positron-lifetime and Doppler-broadening measurements were applied to various point defect structures in Si, GaAs and CdF_2.

In semiconductors, the annihilation characteristics in different defect structures are often rather similar. Therefore, the quality of data is of utmost importance for a succesful analysis. In this work, the stability of the positron lifetime spectrometer was improved in two ways. Techniques to counteract both the random electronic drifts, and the long-term creep related to photomultiplier ageing were developed.

It was found that ageing of the photomultiplier tubes, i.e. nonreversible degradation of the gain, can be slowed down by lowering the operating voltages over the tubes and by compensating the lower gain with fast preamplifiers. This can be done without sacrificing the time resolution on two conditions. First, the voltages in the input electron optics of the tubes must be high enough, and second, the pulse amplitudes at the anodes have to be at least some tens of millivolts. With this method, the lifetimes of the PMTs can be increased at the minimum by a factor of 20.

A scheme to reduce even the fastest drifts of the time zero in the lifetime spectrometer was designed on the basis of a digitally stabilized multichannel analyzer. An artificial reference peak into the spectrum was produced by feeding fast light pulses from a light-emitting diode via two optical fibers of different lengths onto the photomultipliers. In a one-week-long test measurement, drifts of 12 ps were reduced below a level of 0.5 ps.

Positron thermalization at low temperatures was studied in Si and GaAs both experimentally and theoretically. The experiments were based on investigating the temperature dependence of the positron trapping rate at negative vacancy-type defects. In the calculations, the Maxwell-Boltzmann equation was solved for the evolution of the positron momentum distribution. Both experiments and calculations indicate that positron thermalization in GaAs is clearly slower than in Si. According to the calculations, at 10 K in GaAs, the time needed by the positrons to reach twice the thermal energy is 80 ps, whereas in Si it is only 25 ps. The underlying reason for the difference in the thermalization times was found to be in the mass densities of the materials. The positron scattering off longitudinal-acoustic phonons is weaker in heavier hosts than in lighter ones. As a consequence, when analyzing positron annihilation data measured at very low temperatures, the incomplete thermalization may have to be taken into account in some materials.

Vacancy-impurity complexes were investigated in highly n-type silicon by combining positron-lifetime and core-electron momentum distribution measurements. In electron-irradiated As- and P-doped samples, V-As and V-P pairs were observed, respectively. The formation of native V-As_3 complexes was detected when the dopant concentration exceeds 10^{20} cm^{-3}. This is consistent with recent theoretical descriptions of As diffusion [15] and with the idea that V-As_3 plays an important role in the electrical deactivation in heavily As-doped Si.

The optical ionization of the silicon divacancy was studied under illumination with monochromatic light. The positron trapping rate at the divacancies was found to be very sensitive to the photon energy in the range 0.70-1.30 eV. The observations could be explained

in terms of electron and hole emission from the $V_2^{-2/-}$ and $V_2^{-/0}$ levels of the divacancy. The spectral shape of the trapping rate reveals an ionization level at 0.75 eV above the top of the valence band. This was assigned to the $V_2^{-2/-}$ level [16].

In CdF_2, an open-volume defect was observed to be a constituent of the deep-state atomic configuration of the bistable centers, Ga and In. The size of the open volume is at least half of a Cd monovacancy. The positron results are in perfect agreement with recent theoretical calculations predicting two stable configurations for the defects: in the deep state the dopant is in an interstitial position and in the shallow state in a substitutional site [18].

References

1 A. Lietoila, J. F. Gibbons, and T. W. Sigmon, Appl. Phys. Lett. **36**, 765 (1980).

2 K. Saarinen, P. Hautojärvi, and C. Corbel, in *Identification of Defects in Semiconductors*, edited by M. Stavola (Academic, New York, 1998).

3 A. Dupasquier and A. P. Mills jr. (Ed.), *Positron Spectroscopy of Solids*, (IOS Press, Amsterdam, 1995); R. Krause-Rehberg and H. S. Leipner, *Positron Annihilation in Semiconductors*, (Springer, Heidelberg, 1999).

4 M. J. Puska and R. M. Nieminen, Rev. Mod. Phys. **66**, 641 (1994).

5 M. Alatalo, H. Kauppinen, K. Saarinen, M. J. Puska, J. Mäkinen, P. Hautojärvi, and R. M. Nieminen, Phys. Rev. B **51**, 4176 (1995).

6 K. G. Lynn and A. N. Goland, Solid State Commun. **18**, 1549 (1976).

7 K. G. Lynn, J. R. MacDonald, R. A. Boie, L. C. Feldman, J. D. Gabbe, M. F. Robbins, E. Bonderup, and J. Golovchenko, Phys. Rev. Lett. **38**, 241 (1977).

8 K. G. Lynn, J. E. Dickman, W. L. Brown, M. F. Robbins, and E. Bonderup, Phys. Rev. B **20**, 3566 (1979).

9 J. R. MacDonald, K. G. Lynn, R. A. Boie, and M. F. Robbins, Nucl. Instr. and Meth. **153**, 189 (1978).

10 M. J. Puska, C. Corbel, and R. M. Nieminen, Phys. Rev. B **41**, 9980 (1990).

11 C. LeBerre, C. Corbel, K. Saarinen, S. Kuisma, P. Hautojärvi, and R. Fornari, Phys. Rev. B **52**, 8112 (1995).

12 J. Mäkinen, P. Hautojärvi, and C. Corbel, J. Phys.: Condens. Matter **4**, 5137 (1992).

13 J. Mäkinen, C. Corbel, P. Hautojärvi, P. Moser, and F. Pierre, Phys. Rev. B **39**, 10162 (1989).

14 P. Mascher, S. Dannefaer, and D. Kerr, Phys. Rev. B **40**, 11764 (1989).

15 M. Ramamoorthy and S. T. Pantelides, Phys. Rev. Lett. **76**, 4753 (1996).

16 G. D. Watkins and J. W. Corbett, Phys. Rev. **138**, A 543 (1965); J. W. Corbett and G. D. Watkins, Phys. Rev. **138**, A555 (1965).

17 A.I. Ryskin, A. S. Shcheulin, B. Koziarska, J. M. Langer, A. Suchocki, I. I. Buczinskaya, P. P. Fedorov, and B. P. Sobolev, Appl. Phys. Lett. **67**, 31 (1995); R. A. Linke, I. Redmont, T. Thio, and J. D. Chadi, J. Appl. Phys. **83**, 661 (1998).

18 C. H. Park and D. J. Chadi, Phys. Rev. Lett. **82**, 113 (1999).

19 R. M. Nieminen and J. Oliva, Phys. Rev. B **22**, 2226 (1980).

20 A. Perkins and J. P. Carbotte, Phys. Rev. B **1**, 101 (1970).

21 K. O. Jensen and A. B. Walker, J. Phys.: Condens. Matter **2**, 9757 (1990).

22 M. Manninen and R. M. Nieminen, Appl. Phys. A Vol. **26**, 93 (1981).

23 Hamamatsu Photonics K.K., Photomultiplier Tube - principle to application -, 1st edition, (Japan, 1994).

24 B. Leskovar and C.C. Lo, Nucl. Instr. and Meth. **123**, 145 (1975).

25 M. Eldrup, Y. M. Huang, and B. T. A. McKee, Appl. Phys. **15**, 65 (1978).

26 S. Dannefaer, Appl. Phys. A **26**, 255 (1981).

27 B. Somieski, T. E. M. Staab, and R. Krause-Rehberg, Nucl. Instr. and Meth. A **381**, 128 (1996).

28 K. Rytsölä, Nucl. Instr. and Meth. **199**, 491 (1982).

29 Philips Photonics, Photomultiplier tubes, Principles & Applications, (1994).

30 Philips Components, Photomultipliers, Data Handbook, Book PC04, (The Netherlands, 1990).

31 Burle Industries Inc., Photomultiplier handbook, (USA, 1989).

32 J. D. McGervey, J. Vogel, P. Sen and C. Knox, Nucl. Instr. and Meth. **143**, 435 (1977).

33 S.-O. Flyckt, Photonis, private communication (2001).

34 V. H. C. Crisp, I. K. MacKenzie and R. N. West, J. Phys. E **6**, 1192 (1973).

35 J. P. Teixeira Dias, J. Jesus, C. Lopes Gil, and A. P. de Lima, Proceedings of the 8th International Conference on Positron Annihilation, Gent, Belgium, 29 August - 3 September 1988, p. 629.

36 H. Kauppinen, Master's Thesis, Helsinki University of Technology, (1993).

37 P. Kubica and A. T. Stewart, Can. J. Phys. **61**, 971 (1983).

38 P. Kubica and A. T. Stewart, Phys. Rev. Lett. **34**, 852 (1975).

39 E. J. Woll, Jr., and J. P. Carbotte, Phys. Rev. **164**, 985 (1967).

40 J. Mäkinen, C. Corbel, P. Hautojärvi, and D. Mathiot, Phys. Rev. B **43**, R12114 (1991).

41 T. Laine, K. Saarinen, and P. Hautojärvi, Phys. Rev. B **62**, 8058 (2000).

42 K. C. Pandey, A. Erbil, G. S. Cargill III, and R. F. Boehme, Phys. Rev. Lett. **61**, 1282 (1988).

43 D. J. Chadi, P. H. Citrin, C. H. Park, D. L. Adler, M. A. Marus, and H.-J. Gossmann, Phys. Rev. Lett. **79**, 4834 (1997).

44 G. D. Watkins, in *Deep Centers in Semiconductors*, edited by S. Pantelides (Gordon and Breach, New York, 1986), p. 147.

45 S. Kuisma, K. Saarinen, P. Hautojärvi, C. Corbel, and C. LeBerre, Phys. Rev. B **53**, 9814 (1996).

46 U. Piekara, J. M. Langer and B. Krukowska-Fulde, Solid State Communication **23**, 583 (1977); J. E. Dmochowski, J. M. Langer, and Z. Kalinski, Phys. Rev. Lett. **56**, 1735 (1986); J. E. Dmochowski, W. Jantsch, D. Dobosz, and J. M. Langer, Acta Phys. Pol. A**73**, 247 (1988).

47 T. Mattila, S. Pöykkö, and R. M. Nieminen, Phys. Rev. B **56**, 15 665 (1997).

48 J. Mäkinen, T. Laine, K. Saarinen, P. Hautojärvi, C. Corbel, V. M. Airaksinen, P. Gibart, Phys. Rev. Lett. **71**, 3154 (1993).